

Large impact crater histories of Mars: The effect of different model crater age techniques

Stuart J. Robbins^{a,*}, Brian M. Hynek^{a,b}, Robert J. Lillis^c, William F. Bottke^d

^a Laboratory for Atmospheric and Space Physics, 3665 Discovery Drive, University of Colorado, Boulder, CO 80309, United States

^b Department of Geological Sciences, 3665 Discovery Drive, University of Colorado, Boulder, CO 80309, United States

^c UC Berkeley Space Sciences Laboratory, 7 Gauss Way, Berkeley, CA 94720, United States

^d Southwest Research Institute and NASA Lunar Science Institute, 1050 Walnut Street, Suite 300, Boulder, CO 80302, United States

ARTICLE INFO

Article history:

Received 25 June 2012

Revised 6 February 2013

Accepted 25 March 2013

Available online 3 April 2013

Keywords:

Mars
Cratering
Mars, Surface
Asteroids, Dynamics
Magnetic fields

ABSTRACT

Impact events that produce large craters primarily occurred early in the Solar System's history because the largest bolides were remnants from planetary formation. Determining when large impacts occurred on a planetary surface such as Mars can yield clues to the flux of material in the early inner Solar System which, in turn, can constrain other planetary processes such as the timing and magnitude of resurfacing and the history of the martian core dynamo. We have used a large, global planetary database in conjunction with geomorphologic mapping to identify craters superposed on the rims of 78 larger craters with diameters $D \geq 150$ km on Mars, $\approx 78\%$ of which have not been previously dated in this manner. The densities of superposed craters with diameters larger than 10, 16, 25, and 50 km, as well as isochron fits were used to derive model crater ages of these larger craters and basins from which we derived an impact flux. In discussing these ages, we point out several internal inconsistencies of crater-age modeling techniques and chronology systems and, all told, we explain why we think isochron-fitting is the most reliable indicator of an age. Our results point to a mostly obliterated crater record prior to ~ 4.0 Ga with the oldest preserved mappable craters on Mars dating to ~ 4.3 – 4.35 Ga. We have used our results to constrain the cessation time of the martian core dynamo which we found to have occurred between the formation of Ladon and Prometheus basins, approximately 4.06–4.09 Ga. We also show that, overall, surfaces on Mars older than ~ 4.0 – 4.1 Ga have experienced >1 km of resurfacing, while those younger than ~ 3.8 – 3.9 Ga have experienced significantly less.

© 2013 Elsevier Inc. All rights reserved.

1. Introduction

Impact craters are the scars of the primary exogenic planetary modification process throughout the Solar System. Meteoritic bombardment has changed throughout history, likely declining by many orders of magnitude (Neukum et al., 2001 and references therein). The frequency of large impactors – 10s to 100s km – has decreased even more significantly, with very few >100 km-diameter craters having formed in the last few billion years as those impactors were swept up by the planets, ejected from the Solar System, or are in a stable orbit in the asteroid belt or beyond. The exact early cratering history of all bodies in the Solar System is difficult to interpret due to obliteration by later impacts and, except for the Moon, a lack of samples that can be radiometrically dated from regions of known crater densities. For Mars, this history is

further confounded through resurfacing from volcanic, fluvial, and aeolian activity. Large-scale features, such as giant impact craters, are generally the last to be removed by these processes due to their sheer size. Thus, determining the timing of formation of the largest impacts helps elucidate the bombardment history of the planet.

In this work, we have identified 105 large craters with diameters $D \geq 150$ km from a global Mars crater database (Robbins and Hynek, 2012). This work is organized to distinguish between steps of our research that do not require model-dependent analysis – crater measurement – and those that do – age determination. We mapped the rims of the craters that still had visible outcrops and extracted all craters $D \geq 1$ km from the mapped rims (Section 2). We then used various authors' delineations of martian geologic epochs based on $N(16)$ crater densities (areal density of craters $D \geq 16$ km) to examine when these craters formed as a function of geologic time in Section 3. In Section 4, we assign absolute ages to these craters and basins based on both the Neukum et al. (2001) and Hartmann (2005) isochron systems using the Ivanov (2001) impact flux; we also discuss some of the inconsistencies between these methods and our preferred age method based on these

* Corresponding author.

E-mail addresses: stuart.robbs@colorado.edu (S.J. Robbins), hynek@lasp.colorado.edu (B.M. Hynek), rlillis@ssl.berkeley.edu (R.J. Lillis), bottke@boulder.swri.edu (W.F. Bottke).

issues. Section 5 discusses consequences of the computed ages – examining when the martian dynamo ceased, and erosion rates throughout Mars' history.

2. Assigning relative ages from crater densities

2.1. Geologic mapping

The premise of this work is that crater rims will retain the most original record of superposed craters that can be used to derive an age; ejecta blankets will also generally be useful, but it is rare for a large crater on Mars to retain an extensive ejecta blanket. The floors of these features show significant modification on Mars so their surfaces are rarely representative of the formation time of the crater. Ergo, the methodology used here to estimate ages for the large martian impact craters was to map the most original-appearing regions of crater rims and identify the superposed craters. If the large craters also contained a visible ejecta blanket, the ejecta was included as well, and superposed craters were included (this occurred in 4% of cases).

Craters with diameters larger than 150 km were selected from a global martian crater database (Robbins and Hynek, 2012). There are 17 craters identified with diameters between 300 and ~500 km. An additional 28 are in the 200-km range, while 55 are in the 150–200-km range. This was chosen as the cut-off because there were an additional 200 craters in the 100–150 km range and the mapped regions were growing significantly smaller by $D \sim 150$ km. Going down to 150-km-diameter craters ensures inclusion of the 154-km-diameter Gale crater, the landing site of the *Mars Science Laboratory Curiosity* (see Section 4.4). Two basins (where this term is adopted here for craters $D \geq 500$ km) are also included in Robbins and Hynek (2012) due to their relatively sharp remnant rims – Ladon and Prometheus. In addition to these, the most intact rims of Hellas, Argyre, and Isidis were mapped. Fig. 1 shows a map of all the craters examined in this study with the rim outlines carefully traced.

Both image and topography data were used to map the rims of each large crater. Thermal Emission Imaging Spectrometer (THEMIS) data were utilized, specifically the daytime infrared ($12.57 \mu\text{m}$) global mosaic with 100 m spatial resolution (Christensen et al., 2004; Edwards et al., 2011). This dataset covers $\gg 99\%$ of the surface of Mars and was also a basemap for identifying the craters in Robbins and Hynek (2012). Additionally, large craters usually have significant topographic expression so the Mars Orbiter Laser Altimeter gridded dataset ($1/128^\circ$ per pixel (463 m/px) spatial resolution at the equator and up to 512° per pixel near the poles) (Smith et al., 2001) was used to help identify the topographically high rim materials. ArcGIS software was used to digitally map the crater rims, calculate area statistics in a local equal-area projection, and extract included craters for crater spatial-density analysis. The largest craters – Hellas, Argyre, Isidis, and Prometheus – were mapped to closely follow the latest version of the Mars global geologic maps (Tanaka et al., 2012).

Due to the extensive resurfacing history of Mars, mapping crater rims was not always possible. Of the 100 craters < 500 km extracted from the global database, 73 could be mapped and assigned an age in addition to the five basins named above. Other > 1000 km craters – such as Acidalia, Chryse, or Utopia – or the quasi-circular depressions (QCDs) and crustal thin areas (CTAs) of Frey (2008, and references therein) were not included because of their indistinct rims and the lack of certainty that they are impact craters. Mapped examples are illustrated in Fig. 2 (left column) and online Supplemental material (Fig. 7). The mapping approach used often resulted in one or more polygons in an irregular annulus on the topographically highest portions of the rim (Fig. 2 and online sup.). If large craters (i.e., ≥ 50 km) were superposed on the crater rims that were mapped, these large craters were included in the mapping in addition to craters superposed on them and their ejecta (if present). Since complete rims in many cases were not mappable, it is inferred that significant resurfacing has taken place. Therefore, all ages should be considered *minimum* model crater ages.

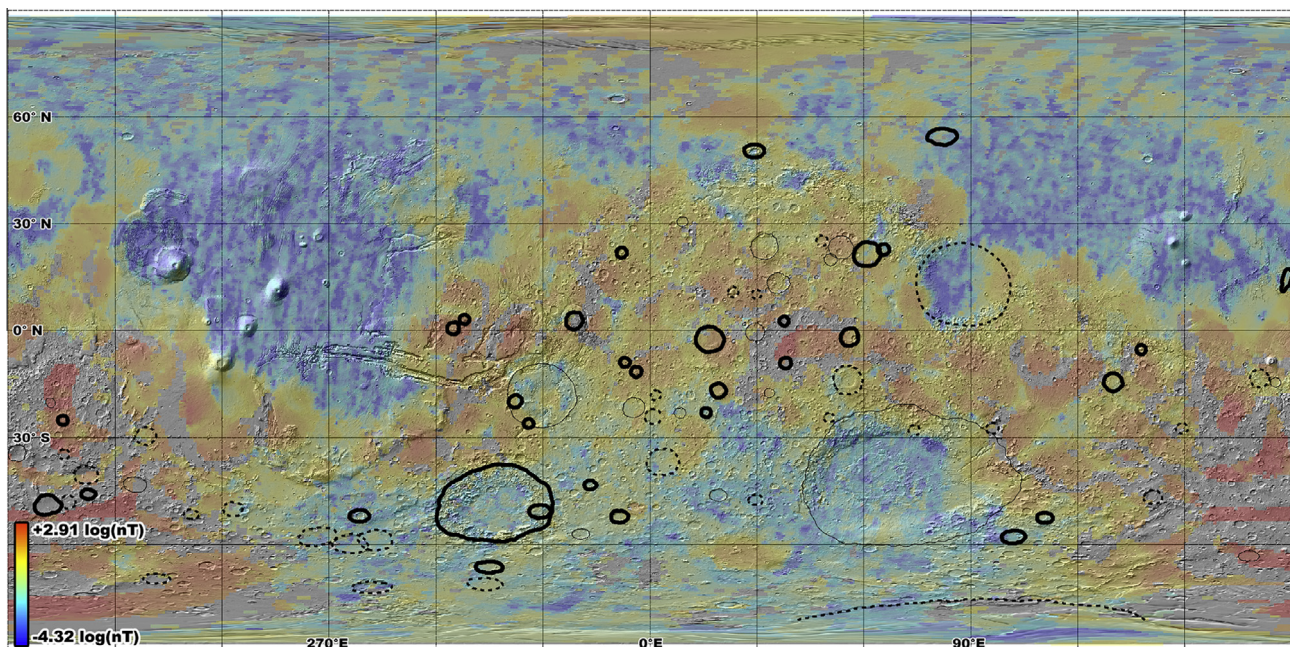


Fig. 1. Locations of all craters $D \geq 150$ km that were dated are outlined in this figure; all rim outlines are hand-drawn and represent the rim crests used to measure diameter. The base layer is MOLA shaded relief (Smith et al., 2001). The colored map on top is reconstructed $|B_{185}|$ magnetic field data (Lillis et al., 2008b). The thickness of the rim outline corresponds with three age groups – thin is older than 4.1 Ga, thick is younger than 3.9 Ga, and the intermediate dashed thickness is intermediate age as determined via the isochron dating method (see Section 4). (For interpretation of the references to color in this figure legend, the reader is referred to the web version of this article.)

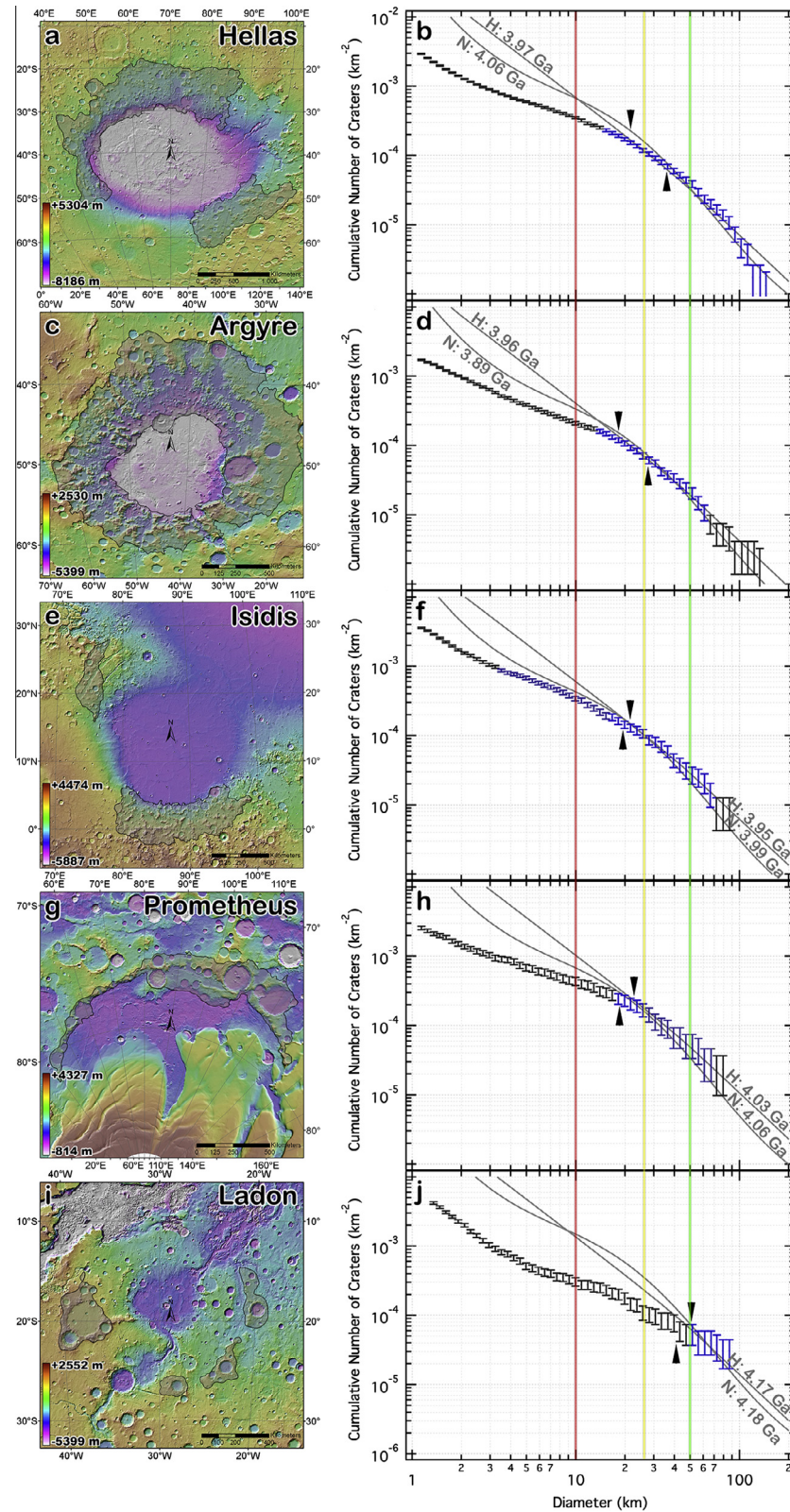


Fig. 2. This paneled figure shows the Hellas (a and b), Argyre (c and d), Isidis (e and f), Prometheus (g and h), and Ladon (i and j) basins and mapping (left column) and the corresponding crater size–frequency distributions (right column) with fitted isochrons overlaid as well as lines indicating where $N(10)$, $N(25)$, and $N(50)$ values are. Additional examples are included in Fig. 7 (online sup.). All graphs show the same scale. Red, yellow, and green vertical lines show the $N(10, 25, 50)$ ages as also color-coded in Fig. 4, while blue data points show the ranges fitted to yield isochron ages. Darker blue points for Prometheus show additional points used when fitting the Hartmann (2005) isochron while those for Isidis were extra points used for Neukum isochrons (Ivanov, 2001). Arrows indicate the isochron turn-off diameter discussed in Section 5.2; upper arrow is turn-off from Hartmann, bottom arrow is turn-off from Neukum. The map projections in the left column are Mollweide except for Prometheus which is stereographic, and the underlying data are MOLA elevation (Smith et al., 2001), while the areas mapped for craters on each basin rim are shown as black-outlined shaded regions. (For interpretation of the references to color in this figure legend, the reader is referred to the web version of this article.)

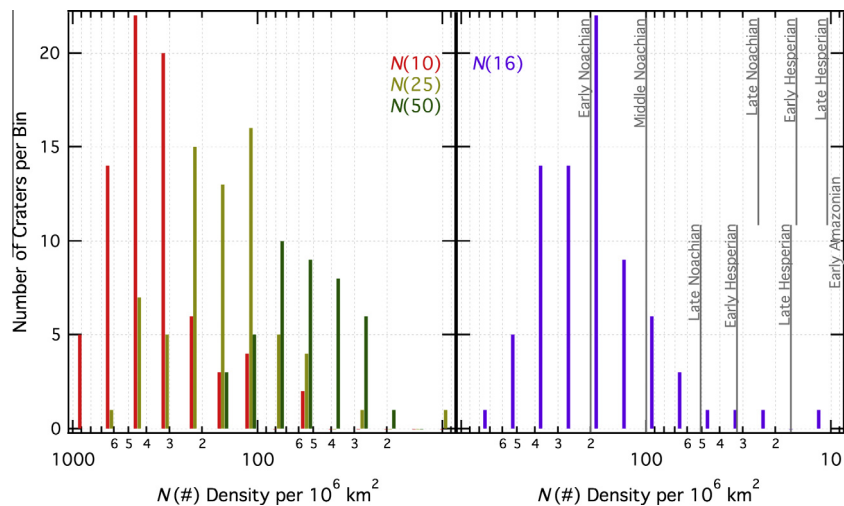


Fig. 3. The $N(D)$ densities of superposed craters on the rims of features dated in this work; only densities that could be determined are displayed (e.g., if a crater did not have a superposed $D = 50$ km crater on the rim, then that is not presented here). Horizontal scale is reversed such that older craters are to the left. Left panel shows $N(10, 25, 50)$ densities, while the right panel shows $N(16)$ densities and the martian epoch cut-offs as given in [Werner and Tanaka \(2011\)](#); full bars are where there is agreement between [Ivanov \(2001\)](#) and [Hartmann \(2005\)](#), lower cutoffs are from [Ivanov \(2001\)](#) and upper are [Hartmann \(2005\)](#). Note that the bins span epoch boundaries and so may include craters on both sides (see [Table 1](#) for actual number of craters in each epoch).

2.2. Size–frequency distributions and crater densities

Crater size–frequency distributions (SFDs) were calculated following the suggestions of the [Crater Analysis Techniques Working Group \(1979\)](#) with some modifications: Craters were binned in multiplicative $2^{1/8}D$ intervals for purposes of slope-fitting. The bins were set as described in [Robbins and Hynek \(2011\)](#), using these standard techniques. An additional feature of the SFD algorithm was run on the incremental SFDs to remove the largest bins with too few craters from display (they are still factored into the cumulative count, just removed from the graph so they are not used in isochron-fitting); this cut-off was set at <3 craters in a cumulative bin to eliminate some issues with small-number statistics in assigning ages. Error bars were calculated by $\pm\sqrt{N}$ Poisson statistics ([Crater Analysis Techniques Working Group, 1979](#)). Once these operations were performed, the incremental SFDs were integrated (discretely summed from largest to smallest) to yield a cumulative SFD (CSFD).

In an effort to eliminate and avoid contamination by secondary craters, isochron-fitting was generally limited to craters $D \geq 10$ km, though in several cases smaller craters had to be used to have enough of a range for decent fitting (e.g., Gale crater, [Section 4.4](#)). In addition, crater morphologies were taken into account to eliminate clear examples of secondary craters from the mapped regions (see discussion in [Robbins and Hynek \(2011\)](#)). The only obvious contamination by secondary craters based on CSFD slope was for $D < 7$ km around Lyot crater and that was because Lyot's ejecta was included.

In relative crater chronologies, many researchers rely on the cumulative crater densities at a fixed diameter as opposed to a range of diameters for isochron-fitting (see [Section 4](#)); this is compactly written as $N(\geq D)$ or $N(D)$ where the D indicates the diameter down to which craters are included in the study. The densities $N(10)$, $N(16)$, $N(25)$, and $N(50)$ were determined for all large craters/basins (if superposed craters of that diameter were available). This range of diameters was chosen so that the smallest, $N(10)$, was directly comparable with [Werner \(2008\)](#) – the only work of similar scope to this study. The largest, $N(50)$, was a compromise between using very large craters that would almost certainly not be secondaries and would be much harder to erase, and the actual existence of $D = 50$ km craters superposed on the larger craters dated. $N(25)$ was selected as a value between 10 and 50 km, approximately in

Table 1

Summary of martian geologic epoch age estimates and the number of craters dated in this work that are from each.

Epoch	Time, Ga (I01) ^a	Time, Ga (H05) ^b	#Craters (I01) ^a	#Craters (H05) ^b
Early Noachian	>3.97	>3.96	51	51
Middle Noachian	3.86–3.97	3.85–3.96	20	20
Late Noachian	3.74–3.86	3.57–3.85	4	6
Early Hesperian	3.65–3.74	3.40–3.57	1	0
Late Hesperian	3.46–3.65	3.00–3.40	1	1
Early Amazonian	1.45–3.46	0.880–3.00	1	0
Middle Amazonian	0.387–1.45	0.235–0.880	0	0
Late Amazonian	<0.387	<0.235	0	0

^a I01 refers to [Ivanov \(2001\)](#) chronology used in the Neukum system, related in [Werner and Tanaka \(2011\)](#).

^b H05 refers to [Hartmann \(2005\)](#) chronology related in [Werner and Tanaka \(2011\)](#).

the middle of a logarithmic progression between the two. $N(16)$ was included only so that the craters could be placed into the chronology of the Mars global geologic maps, after [Tanaka \(1986\)](#) and revised by [Werner and Tanaka \(2011\)](#) for the new Mars global geologic maps ([Tanaka et al., 2012](#)) (the epochs are only defined for $N(0.1, 1, 2, 5, 16)$ in [Werner and Tanaka \(2011\)](#)).

3. Distribution of crater densities in martian geologic time

Often when dating geologic surfaces, the density of craters per unit area are used as an across-the-board comparison to determine relative ages. [Fig. 3](#) shows histograms of the $N(10, 16, 25, 50)$ densities with the martian epochs overlaid on the $N(16)$ histogram (right panel). The histograms show a rapid increase of number of craters from large densities towards small until a peak is reached, and then there is a more gradual decline in number of craters as lower superposed densities are reached. This indicates that few very old crater rims are still preserved today, while the actual densities have been interpreted as a rapid decrease in the cratering rate early in Mars' history ([Fig. 3](#), right panel).

There was good internal agreement in assigning martian epochs to these craters using three different $N(16)$ density systems: (1) from [Tanaka \(1986\)](#), (2) the [Ivanov \(2001\)](#), and (3) [Hartmann](#)

(2005) systems presented in Werner and Tanaka (2011). These are detailed in Table 1. As listed, only three craters were classified in different epochs – Bakhuisen (Late Hesperian versus Late Noachian), Galle (Early Hesperian versus Late Noachian), and Lyot (Early Amazonian versus Late Hesperian). This shows that despite some fundamental differences between the generally two competing systems – the Hartmann chronology (Hartmann, 2005) and Neukum chronology (Neukum et al., 2001) – when placing general epoch boundaries on features, there is good agreement.

Comparison with Werner (2008) was done based on the $N(10)$ ages reported in that work with the percentage uncertainty reported for $D \approx 10$ km in the tables in that work's Appendix A. Of the 19 craters that were mapped both in that study and this, 9 agree within each others' 1σ uncertainties while 10 disagree. Within the disagreements, there is no uniform offset based on age, and fully half have lower density in these counts and half have lower density in the Werner (2008) counts. The magnitude of the disagreements are also random, with some as much as a factor of $2\times$ difference, while two are different by $\approx 20\%$ but that is outside the respective 1σ uncertainties.

There is better agreement between the actual crater model age estimates (see Section 4.4), but determining why there are differences in the more basic measurement – superposed crater density – is a more fundamental question. From examination of the mapping, there are several disagreements, even for seemingly distinct crater rims. For example, Gusev was mapped here with a thin annulus around the rim (Fig. 7g), and the $N(10)$ density was 1170 ± 390 per 10^6 km². The mapping in Werner (2008) includes regions out nearly a full crater diameter to the south and east beyond the crater rim, and $N(10)$ was 606 ± 121 per 10^6 km². The $N(10)$ difference is very likely due to the mapping, and the preferred interpretation here is that study included some significantly resurfaced terrain, lowering the overall age for Gusev. Beyond the mapping likely contributing the most to the differences, Werner (2008) also relied on Viking MDIM mosaics rather than the latest, usually clearer and higher resolution, data from THEMIS mosaics on which to identify superposed craters. Robbins and Hynek (2012) showed that relying on these older data can result in some false positive crater identifications and a myriad of false negatives (missed craters).

It is not possible at this point in the discussion to provide a preferred age method, for there are limitations to any preference. For example, and as will be discussed later, it is generally preferable to use the largest craters when relying solely on an $N(D)$ age because these are the least likely to have experienced erasure since the features formed. However, this is not always possible, and it is impossible with this study when wanting to place the craters into martian chronostratigraphic epochs that are only defined for certain crater diameters (e.g., $N(16)$ was used in this case). Meanwhile, the corresponding absolute ages for each of the martian epochs has been and still is a subject of much study over the years (i.e., the systems mentioned above all have somewhat different boundaries). For that reason and those discussed in Sections 4.1 and 4.2, we reiterate that there are uncertainties associated with absolute ages derived from crater chronologies. With those uncertainties in mind, we calculate the model-based absolute ages to enable comparison with other analyses and to evaluate consistency of the current understanding of the martian chronology.

4. Ages of $D \geq 150$ km craters

4.1. Assigning crater-based absolute model ages

Two isochron systems were used in this work both for comparison and validation purposes: the Hartmann and Neukum systems.

The ages are presented side-by-side, despite often differing, because at the present time neither one is preferred over the other in the planetary community. Neukum isochrons were based on the 11th-order polynomial function described in Ivanov (2001) to the precision listed in Werner and Tanaka (2011). This system is based on a non-linear least-squares fit to lunar mare counts (Neukum, 1983) and is a CSFD. The function is scaled through time based on the function presented in Ivanov (2001) that calculates the $D = 1$ km density based on the time of interest, using the impact flux through time derived from scaling of Apollo and Luna sample returns (e.g., Stöffler and Ryder, 2001). Isochron shape does not change based on age, only the crater density (vertical offset in the plots), which is a subject of debate (see Section 4.2 and, e.g., Strom et al. (2005)). The time-scaling function is:

$$N(D \geq 1 \text{ km}) = 2.68 \times 10^{-14} (e^{6.93T} - 1) + 4.13 \times 10^{-4} T \quad (1)$$

where T is time before present in billions of years.

The Hartmann system is based on Hartmann (2005) with several corrections (due to typos in the original paper) and one modification. First, the three-part power laws described in Hartmann (2005) were used to construct a piece-wise incremental isochron for a 3.5 Ga old martian surface from 0.5 to 1024 km in $2^{1/2}D$ intervals with the listed correction for atmospheric filtering. The power laws were used because the table values given are offset and missing the $D = 2$ km point such that values for $D > 1.414$ km are off by one diameter bin (W. Hartmann, personal communication via C. Fassett, personal communication). This incremental isochron was then scaled by $5.72^{-1}\times$ (as opposed to the misprinted $5.76^{-1}\times$), as validated by the time-scaling function in the paper to create a 1 Ga isochron to use as a model. The only modification from Hartmann's (2005) incremental function was to then integrate from large to small diameters to create a cumulative isochron. The time-scaling function from the 1 Ga model isochron used is from Ivanov (2001).

Two methods were used to assign *minimum* model crater ages to the large craters and basins within both the Hartmann and Neukum chronologies. The first was to convert the $N(D)$ densities to an age using the scaling functions described above. The second method is an isochron fit: A range of diameters from each crater's CSFD was selected that paralleled the isochron function. Other diameter ranges that did not parallel were assumed to be affected by resurfacing (erosion, infilling, etc.), incomplete counts, or other non-age-related issues (see blue points, Fig. 2, right column). An algorithm was written to calculate the average difference between the CSFD points and the model 1 Ga isochron, weighting each point the same. Using the time scaling function (Ivanov, 2001), it then determined the age that best fit the selected diameter range. Age uncertainties were determined by taking the formal \sqrt{N} error bars at each diameter bin used in the fitting and first adding them to the CSFD data point. The best-fit isochron for the new CSFD was then calculated. The same procedure was followed except the uncertainty was subtracted from the original CSFD points. The original model isochron age was then subtracted from these new fitted ages to estimate the plus/minus uncertainties in each determined age. Due to the nature of the time scaling function, model ages younger than ~ 2.5 Gyr have symmetric uncertainties and older ones generally have larger negative uncertainties than positive (e.g., $3.5^{+0.2}_{-0.4}$ Ga versus 2.0 ± 0.3 Ga). Note that this is different from the popular CraterStats tool distributed by Frie Universität Berlin (Michael and Neukum, 2010) which estimates uncertainty only based upon the $D = 1$ km point's uncertainties (consequently, uncertainties calculated here are generally larger). However, ages fit by this technique generally agree with that tool.

These statistical uncertainties are in addition to the issues correlating lunar crater ages with lunar sample return absolute ages

Table 2
Data summarizing the ages calculated in this work for several of Mars' largest basins. Top line is Hartmann chronology (Hartmann, 2005), bottom line is Neukum chronology (Ivanov, 2001); both use the Ivanov (2001) time scaling function. Data for the large craters are included as [online Supplemental material](#).

Basin	Mapped area (km ²)	N(10) ^a	N(16) ^a	N(25) ^a	N(50) ^a	N(10) age ^b (Ga)	N(16) age ^b (Ga)	N(25) age ^b (Ga)	N(50) age ^b (Ga)	Isochron age ^b (Ga)	Age (NT05 ^c) (Ga)	Age (F08 ^d) (Ga)	Age (W08 ^e) (Ga)	Age (FH11 ^f) (Ga)	Turn-off, D (km)
Argyre	1.5 × 10 ⁶	204 ± 12	132 ± 10	71 ± 7	21 ± 4	3.78 ± 0.01	3.85 ± 0.01	3.88 ± 0.02	3.91 ± 0.03	3.96 ± 0.02	4.04	4.04	3.83 ± 0.01	3.92	13
Hellas	2.3 × 10 ⁶	333 ± 12	211 ± 10	117 ± 7	35 ± 4	3.86 ± 0.01	3.93 ± 0.01	3.96 ± 0.01	3.99 ± 0.02	3.97 ± 0.02	4.08	4.07 ± 0.05 ^g	3.99 ± 0.01	4.02	34
Isidis	4.7 × 10 ⁵	329 ± 27	185 ± 20	108 ± 15	29 ± 8	3.86 ± 0.01	3.91 ± 0.02	3.95 ± 0.02	3.96 ± 0.04	3.95 ± 0.03	3.93	3.81	3.96 ± 0.01	3.97	20
Ladon	8.0 × 10 ⁴	288 ± 42	213 ± 36	110 ± 26	55 ± 18	3.84 ^{+0.02} _{-0.03}	3.92 ^{+0.02} _{-0.03}	3.95 ^{+0.03} _{-0.04}	4.06 ^{+0.04} _{-0.06}	4.17 ^{+0.05} _{-0.08}	4.04	4.15 ± 0.05 ^g	3.96 ± 0.01	3.96	20
Prometheus	1.3 × 10 ⁵	416 ± 57	281 ± 47	171 ± 36	56 ± 21	3.90 ± 0.02	3.98 ^{+0.02} _{-0.03}	4.02 ^{+0.03} _{-0.04}	4.06 ^{+0.05} _{-0.07}	4.03 ^{+0.04} _{-0.05}	[Age not reported elsewhere]				
						3.99 ± 0.02	4.03 ^{+0.02} _{-0.03}	4.06 ^{+0.03} _{-0.04}	4.14 ^{+0.05} _{-0.07}	4.06 ^{+0.04} _{-0.05}	[Age not reported elsewhere]				

^a N(D) densities are 10⁶ km⁻² and are cumulative, reflecting all craters ≥ D.

^b This work.

^c NT05 refers to Nimmo and Tanaka (2005). Uncertainties were not given.

^d F08 refers to Frey (2008). Uncertainties were not given in this paper.

^e W08 refers to Werner (2008).

^f FH11 refers to Fassett and Head (2011). Uncertainties were not given.

^g Uncertainty in Hellas' age as well as the age and uncertainty for Ladon are given in Lillis et al. (2008a, 2008b).

and then extrapolating to Mars based on its surface gravity, proximity to the asteroid belt, impactor velocities at ~1.4 AU, and other scaling differences (Ivanov, 2001) which themselves are estimated at present to be accurate to within a factor of ~2× (Neukum et al., 2001; Hartmann, 2005). The main literature comparisons quote ages to the 1 or 10 Myr level (Nimmo and Tanaka, 2005; Werner, 2008; Fassett and Head, 2011); specific ages in this paper are given to the 10 Myr level while combined results are given to the 100 Myr level – however, it is recognized that the inherent uncertainties in the isochrons are larger than this in every case. Despite these, if one can assume similar geologic and environmental processes, the *relative* chronologies from the crater densities are still accurate; that is, a surface dated here to 3.5 Ga will be younger than one dated to 4.0 Ga when absolute age dating can be done.

4.2. Inconsistencies and difficulties with the technique

There are several issues when using craters to age-model surfaces on Mars, and the first can be shown simply by examining the *N(D)* densities in [Tables 2](#) (in paper) and [3](#) (online sup.). If the same crater population formed on all terrains and the same crater population were removed on all terrains, then the ratio of, e.g., *N(10)/N(16)*, should be the same for all 78 craters in this study. Instead, it ranges between 1.08 and 5.47 with a median 1.55 ± 0.43 (±28%) average deviation. *N(25)/N(16)* ranges 0.32–0.90 with a median 0.61 ± 0.11 (±18%), and *N(50)/N(16)* ranges 0.094–0.58 with a median 0.25 ± 0.08 (±31%). A direct consequence of this with regards to comparison with other work, or even using *N(D)* densities as dating methods, is that they are not inter-comparable. For example, work using *N(300)* densities to assign ages (e.g., Frey, 2008) or *N(200)* (e.g., Nimmo and Tanaka, 2005; Werner, 2008) can result in very different ages from the *N(10)* ones detailed here. Similarly, *N(1)* densities reported in Werner (2008), if converted to and used as model ages, can result in significant differences.

Additionally, they are not internally consistent, such that the relative chronology between terrains can change when using a different diameter. To use an extreme example, this could mean that a volcanic flow and valley network may show the lava to have formed before the valley when using *N(1)*, but the valley formed before the lava when using *N(0.1)*. This means that the technique cannot be blindly applied. (Though, in most cases the relative uncertainties in densities do overlap this range of difference.)

This also translates into a lack of consistency within a given isochron system, for isochron shapes do not change with age – they only differ in overall density: When converting a *N(D)* to an absolute model crater age, unless the crater SFD parallels the isochron function over the full range of crater diameters used, different ages will result. And, since the Hartmann function is different from the Neukum function, the ages found will *always* differ between different *N(D)*s in at least one of the two systems. This issue is well illustrated in the SFDs of [Fig. 2](#) (right column) and the distribution in [Fig. 4](#) (top), where the four different ages (three *N(D)* and the isochron fits) yield different results and they are not always in each others' uncertainty range. [Fig. 2](#) (right column) also shows that crater SFDs will rarely follow a given isochron function over a large diameter range. Researchers will often pick a chronology they trust (Hartmann or Neukum) and then a diameter range they think parallels it best; this “art form” is likely why the *N(10)* ages between this work and Werner (2008) disagree in 10 of 19 cases and the disagreement is split evenly between older and younger densities, whereas the ages calculated only disagree in six cases (when including basins) and the ages here are all older (see Section 4.4).

These systems also explicitly require that the size–frequency distribution of impactors be constant throughout time. Although there is no consensus within the community, several works have suggested that there existed at least one different impactor

population prior to the time of the Late Heavy Bombardment at Earth ~ 3.8 – 4.0 Ga (i.e., Strom et al., 2005; Fassett et al., 2012). If this hypothesis is correct, and if the populations at Earth were the same at Mars, then comparing $N(D)$ densities for martian craters older than ~ 4 Ga versus those younger than ~ 4 Ga is not as meaningful.

Another issue with using $N(D)$ ages is well illustrated in Fig. 4 where the impact flux peak is pushed progressively to younger ages as smaller $N(D)$ sizes are used, but fewer features can be dated with larger $N(D)$ because of the decreasing likelihood of an impact of that size. This is because the crater SFDs often fall below isochrons at smaller diameters due to what is generally interpreted as resurfacing. A case-study of Hellas basin (Fig. 2a and b) shows this well where the isochrons were fit between $15 < D < 150$ km craters and so match the $N(50)$ age well. But for $D < 35$ km, the SFD in practice follows the general shape of the Neukum isochron but it is depressed, resulting in progressively younger $N(25)$, $N(16)$, and $N(10)$ ages (Table 2). Since the Hartmann isochron has a shallower slope in this particular diameter range, the SFD follows it better, until about $D = 20$ km, resulting in more consistent $N(25)$, $N(50)$, and isochron-fit ages under that chronology. Results from Ladon basin (Fig. 2i and j) emphasize where one will get a significantly different $N(10)$ age from $N(50)$ due to resurfacing. Consequently, one should not use $N(D)$ densities indiscriminately, for erosion and resurfacing can remove craters to result in an anomalously younger age.

The effect is significant in the case of the impact flux (Fig. 4, top), pushing the peak at $N(50)$ from ~ 4.1 – 4.2 Ga to ~ 3.9 – 4.0 Ga for $N(10)$. However, this in itself is an artifact because it does not represent an actual sampling of the large craters dated: Only 33 craters were dated via $N(50)$, 59 were dated with $N(25)$, and all 78 mapped craters/basins were dated with $N(10)$. Because all craters and basins examined had $D \sim 10$ km craters while not all had $D \sim 50$ km craters superposed, this also meant that the isochron fitting in general was weighted towards smaller craters.

In comparison, the method used by Nimmo and Tanaka (2005) was $N(200)$ ages from the work of Frey (2004). Frey (2008) also used large QCD superposed ages, while Werner (2008) and Fassett and Head (2011) used the isochron method, the former using Neukum-based isochrons and the latter using both systems. This is discussed further in Sections 4.3 and 4.4 where the preferred method from this work is discussed.

4.3. Ages – basins

Significant work exists describing and attempting to date the large martian basins, especially Utopia, Hellas, Acidalia, Chryse, Argyre, and Isidis (e.g., Wilhelms, 1973; Schultz et al., 1982; Schultz and Frey, 1990; Nimmo and Tanaka, 2005; Frey, 2008; Werner, 2008; Fassett and Head, 2011). The technique and database discussed above were applied to three of these (Hellas, Argyre, and Isidis) as well as Ladon and the south polar Prometheus basins, two that have not previously been extensively mapped and dated. A summary of results from this work compared with several recent estimates (Nimmo and Tanaka, 2005; Frey, 2008; Werner, 2008; Fassett and Head, 2011) is listed in Table 2. The mapping and crater SFDs with isochrons for Hellas, Argyre, Isidis, Prometheus, and Ladon are shown in Fig. 2. The general agreement of ages with these previous works lends support for this technique and the ages calculated for the smaller craters. The large surface areas mapped and the few basins examined permit further exploration into (a) the uniformity of mapped surfaces, and (b) whether the different ages found are actually different.

Towards the first point, a question arises of whether the different regions of a mapped crater rim are self-similar, or if they reveal different ages individually that average to a single age that is then quoted. To explore this, the different polygons representing the rim

of Hellas (two polygons), Isidis (two polygons), and Ladon (four polygons) were each analyzed individually and $N(50)$ densities per 10^6 km² were calculated. The two Hellas rim sections each had a density 38 ± 8 and 34 ± 4 , while the aggregate was 35 ± 5 . The two Isidis rim sections each had a density 33 ± 18 and 29 ± 8 , while the aggregate was 29 ± 8 . The Ladon rim sections were 49 ± 36 , 63 ± 47 , 85 ± 71 , and 71 ± 29 , and the aggregate was 55 ± 18 . From this, one can see that the rim sections are generally similar in age and there are not statistically significant differences between them.

Towards the latter point, Table 2 presents numerous different age estimates that are difficult to interpret and appear to be inconsistent. For example, the ages assigned based on $N(50)$ densities under both chronology systems place the order of basin age (oldest to youngest): Prometheus, Ladon, Hellas, Isidis, Argyre. The difference between Prometheus and Ladon is only 0.01–0.02 Gyr, well within their uncertainties. Meanwhile, the isochron-based ages under the Hartmann system transpose several: Ladon, Prometheus, Hellas, Argyre, Isidis. The difference between Ladon and Prometheus is 0.04 Gyr and Argyre and Isidis 0.01 Gyr. But, the Neukum-based ages place the order at: Ladon, Prometheus/Hellas (same), Isidis, Argyre; the difference in age between Isidis and Argyre with this system is 0.10 Gyr with uncertainties on the ages of only 0.02 Gyr. The question of which one should “believe” or use, or what one can conclude, is an important one when confronted with this type of conflicting data.

The first stand – picking a system, Hartmann (2005) or Neukum et al. (2001) – is not one that can be taken at this time. At present, all that can be said is that there are two systems that each have merits and problems, and based on this work we cannot recommend one over the other. The second stand – isochrons versus $N(D)$ – is easier to address from the authors’ point of view: Isochrons are likely to yield a more accurate age estimate than a single $N(D)$. Fitting a CSFD to isochrons makes use of more of the crater data and generally eliminates the problem of picking individual diameters from which to measure an age, where the diameter chosen may be a poor representation due to resurfacing or erosion. If one must use $N(D)$ values to estimate an age, it is recommended that the larger diameters are more likely to be accurate because they will have experienced the least erasure.

With this in mind, the formal uncertainties are also important to examine. In all four of the scenarios ranking these five large craters, Hellas was in the middle. But, the uncertainties in the age estimates generally overlapped with Isidis, or even Prometheus and Ladon. The only way to shrink the uncertainties from this technique is to have more craters, which requires either more time to have passed or to use a larger surface – neither of which are feasible. Ergo, one returns to the question of which order to trust and if the ages are distinct? First, the isochron-based ages, rather than $N(D)$ -based, are most likely to be most accurate, so Ladon is likely the oldest of the five basins with Prometheus next, but the formation time between it and Hellas is too small to statistically resolve with this technique. Regarding whether Isidis or Argyre is younger, given that the $N(50)$ density puts it as older, and the difference between Argyre and Isidis is only 0.01 Gyr under the Hartmann chronology, it is likely that Isidis is older than Argyre, making Argyre the youngest >1000 km-diameter crater on Mars. And, while the uncertainties could put Hellas as older than both Ladon and Prometheus or younger than Isidis, the most consistent story between this and other (stratigraphic) techniques places Hellas as intermediate among these five.

4.4. Ages – large craters

The only comparable work age-modeling the large craters in this study ($D < 500$ km) was performed by Werner (2008). The ages

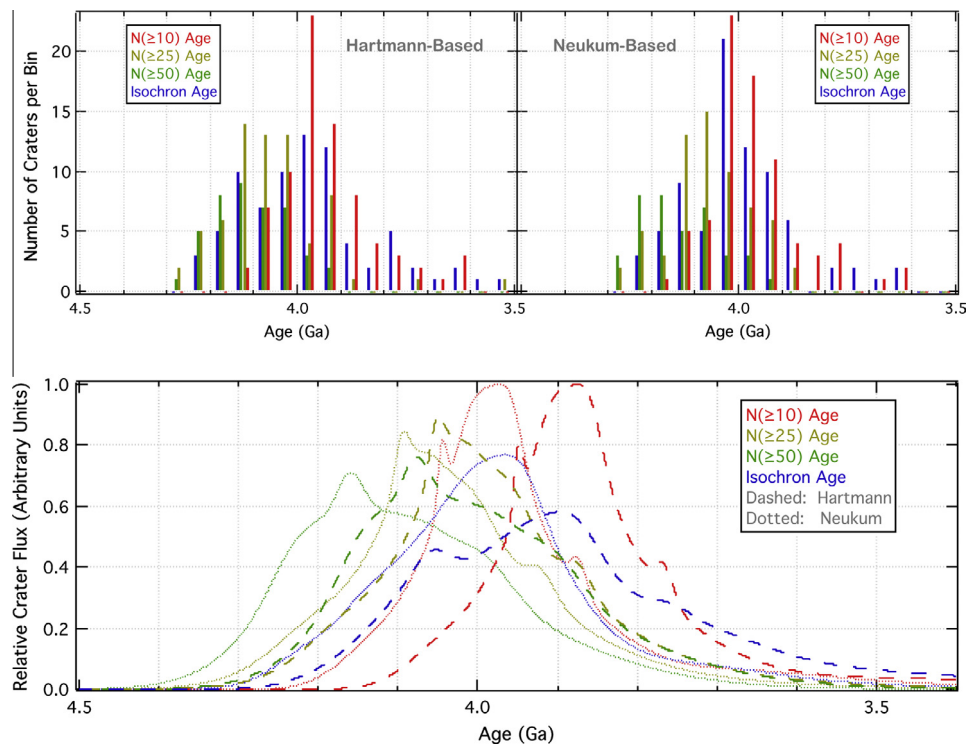


Fig. 4. Top – raw binned data from both the Hartmann (left) and Neukum (right) chronologies for all craters in this study (Table 2 and online sup.). Data are shown from using $N(10, 25, 50)$ and isochron-fitting ages and color-coded per the right column of Fig. 2. The different methods are slightly offset within each 50 Myr-wide bin so they are visible. Bottom – Model impact flux curves (ideograms, or probability distributions) based on each crater age for the different techniques and chronologies (see Section 4.2 for how these were computed). There was no offset for clarity in this panel, and it clearly shows a systematic preference for younger ages with smaller diameters used for $N(D)$ (see Section 4.5). (For interpretation of the references to color in this figure legend, the reader is referred to the web version of this article.)

calculated here statistically agree with those from Werner (2008) except in four cases when using the Neukum-based ages (Antoniadi, Kepler, Lowell, and Gusev); all craters from Werner (2008) overlap at least one of the Hartmann-based ages in this work. In all cases of Neukum-based age disagreement, an older age was calculated here. For Antoniadi and Gusev, the ages are still quite close and would overlap should the uncertainties in the ages by Werner (2008) increase from 10 Ma to 30 Ma and 40 Ma, respectively (representing what many would consider a more reasonable uncertainty estimate). The largest discrepancy with the Neukum-based age is Lowell where the ages differ by approximately 150 Ma, older in this work. Examining the mapping by Werner (2008) of Lowell, the techniques were different than most other craters in that paper and those discussed above, including the entire crater cavity in the mapping as opposed to just the rim and some surrounding ejecta (see Fig. 7o, online sup.). The different datasets used (Viking versus THEMIS and MOLA) as well as the area difference to include a potentially resurfaced crater floor (larger area, fewer large craters) are more than enough to account for the disparate ages between the works.

Internal consistency with any mapping and age-modeling system is important, and there were several pairs of large craters that physically overlapped each other that were dated. The ages were determined blindly and only compared afterwards. The Greek and English letter names refer to craters listed in Table 3 as online Supplemental material:

1. Huygens, Savich, and Terby are on top of Hellas' rim. The derived ages of these three craters are younger than Hellas, though Huygens and Savich overlap Hellas' error bars.
2. Antoniadi rim and ejecta material are on top of Crater η (23.5°N, 53.2°E), supporting the determination Antoniadi is ~ 300 Ma younger. Schöner and Flammarion are also emplaced

on Crater η , and they were both found to be younger (Schöner nearly the same age to ~ 30 Ma younger, and Flammarion by ~ 200 Ma).

3. Galle is emplaced on Argyre, supporting its younger age of ~ 300 Ma.
4. Vindograv is emplaced over Ladon, and Vindograv was found to be ~ 200 – 300 Ma younger. Similarly, Holden is emplaced over Ladon and was found to be ~ 350 – 650 Ma younger.
5. Copernicus overlies Crater I (-48.3°N , -163.3°E) and an age difference of ~ 60 – 120 Ma was found; again, the stratigraphy supports the relative ages.
6. The stratigraphy of Baldet over Antoniadi supports the relative ages of Baldet ~ 50 Myr younger.

As discussed earlier, the inherent uncertainties in the ages are likely larger than a few 10s Myr, so whether, i.e., Baldet's younger age of ~ 50 Myr than Antoniadi is meaningful is debatable. However, that debate is not meant to be a part of this work, especially because it is likely unresolvable with current data. What is important and reassuring for the technique is that the derived age of Baldet is younger than Antoniadi, and the mapping relations confirms the relative age relationship from superposed rim craters.

Of particular interest to the Mars community is Gale crater, a 154-km-diameter crater located at -5.4°N , 137.8°E and the landing site of the Mars Science Laboratory Curiosity. The crater has been estimated to be Noachian in age, with previous work placing it ~ 3.5 – 3.8 Ga (Greeley and Guest, 1987; Cabrol et al., 1999; Thompson et al., 2011). The work described in this paper places it squarely in the Middle Noachian epoch with an $N(16)$ density of 171 ± 131 craters $D \geq 16$ km per 10^6 km 2 . With the large uncertainty due to few large superposed craters, the $N(16)$ density could place it from Early Noachian to Late Noachian (Hartmann) or Early Hesperian (Ivanov) under the system described in Werner and Tanaka

(2011). If smaller craters are used, the $N(5)$ density is 476 ± 221 , placing it in the Middle Noachian (Hartmann) or Late Noachian (Ivanov); with the uncertainty factored in, it remains in the Middle Noachian under Hartmann but could be Late to Middle Noachian under Ivanov. $N(2) = 1402 \pm 381$ places it in Late Noachian. This is the smallest $N(D)$ that can be used for Gale and still derive a somewhat consistent age with larger $N(D)$ s for Gale – the isochron fits were done between 2 and 9 km; above this, there is only one superposed crater, and below this, the CSFD falls well below both isochron systems. When using isochron-based fits, this work places Gale at $3.89^{+0.05}_{-0.08}$ Ga under the Neukum isochrons and $3.68^{+0.07}_{-0.12}$ Ga when using Hartmann isochrons – ages that do not overlap – and place Gale's formation in the Middle Noachian and Early Hesperian, respectively. The lack of overlap and 210 Myr difference is because the isochrons were fit over a diameter range that the two systems disagree the most.

Given these estimates, and despite its probable Noachian age, Gale is among the youngest large craters dated in this work; it has the 20th youngest $N(16)$ density and 12th youngest $N(10)$ density; the isochron-based ages place it 13th youngest under both Hartmann and Neukum isochrons out of the 78 craters dated. As mentioned previously in this paper, the exact ranking is open to debate and actually irrelevant for this discussion – the conclusion to be drawn is that the various rankings are consistent with it being in the youngest 20–25% of large craters to have formed on Mars, and so processes that affected it must have happened after the first ~600–800 Myr of martian history.

4.5. Impact flux

In the top left panel of Fig. 4 is illustrated the raw histogram of ages from Hartmann-based chronology while the top right shows the same from the Neukum-based chronology for $N(10, 25, 50)$ densities; $N(16)$ were not included for clarity. The bottom plot shows a set of ideograms – probability distributions from the ages (Solow, 2002). These were calculated by examining each age (via each method) individually. A piece-wise Gaussian was created with a mean at the age determined, the older side having a standard deviation matching the positive uncertainty, and the younger side of the Gaussian with a standard deviation matching the negative uncertainty. The two halves were matched such that they were continuous at the mean. The overall Gaussian was then normalized to have an area of 1. All the Gaussians for each individual age method were then summed to be the curves shown in Fig. 4, yielding an impact flux distribution. This technique acts to smooth the

raw histogram, emphasize well-defined ages, and diminish the impact of ages with a large uncertainty.

At this point, the pattern alluded to in Section 4.2 bears reemphasis: Due to resurfacing and other crater erasure processes, there is a marked pattern of progressively younger ages when using $N(\text{smaller})$ diameters. Additionally, because few craters have $D \sim 50$ km craters superposed, isochron fitting resulted in ages generally between $N(10)$ and $N(25)$ because that was the region of the CSFDs that best paralleled the isochron functions and did not show evidence of crater erasure.

Neither the raw nor the smoothed ages show a flux distribution that would be expected from (1) a decline from planet formation, (2) a spike from the Late Heavy Bombardment, and (3) the subsequent decline in cratering; however, since the Ivanov (2001) chronology does not include an LHB spike, it should not be surprising that one was not found. Anchoring a few absolute ages would be necessary to determine the actual impact flux to be used to calibrate the ages presented in Fig. 4 and Tables 2 and 3 (latter is online sup.). What this figure does show is that, even though there are offsets with different $N(D)$ -based ages, the overall shapes are generally similar. This reemphasizes the point that as an ensemble, the ages tell the same general history of large martian impacts.

5. Geophysical implications

5.1. Global and local magnetic field

Lillis et al. (2008a) examined the magnetic field at 185 km altitude ($|B|_{185\text{km}}$) found within 0.5 radii of the basin's center (innermost 25% of the basin's area) and compared with $N(300)$ age estimates from Frey (2008) for 20 basins $D > 1000$ km. They found that the youngest five basins studied (Argyre, Isidis, Hellas, Utopia and North Polar) all have extremely weak magnetic fields comparable to or below the noise level of 3–4 nT in the magnetic mapping technique, whereas the other 15 (older) basins all contain substantial crustal fields. This established that a cessation in post-impact crustal magnetization (and hence likely dynamo activity) occurred around $N(300) = 2.6 \pm 0.5$, which corresponds to 4.12 Ga in absolute model age. Very few of those craters used have clear, mappable rims and so were not used in this work.

The ages derived for craters in this work allows a magnetic/age re-examination of three of these demagnetized young large craters, as well as Prometheus and Ladon, which were not considered by Lillis et al. (2008a). Ladon is unambiguously magnetized ($|B|_{185\text{km}} = 42$ nT), as shown by Lillis et al. (2008b), where the

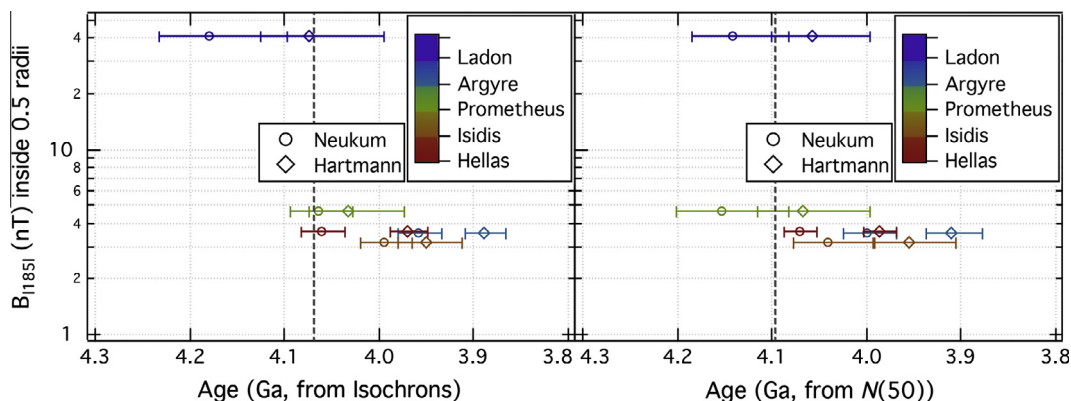


Fig. 5. The magnetic field within the innermost 25% of each basin's area is plotted against the ages for both the Hartmann (2005) and Neukum et al. (2001) isochron systems for both isochron- and $N(50)$ -based ages. Results show that Ladon is the only magnetized basin (see Section 5.1, and Lillis et al. (2008a)), indicating that the magnetic field of Mars likely ceased between its formation and that of the other dated basins. The vertical dashed line in both frames show the average between the oldest age for Prometheus and Ladon, which is when we place this transition. The very close tight overlap for the isochron-based ages and complete overlap for the $N(50)$ ages is discussed in Section 5.1.

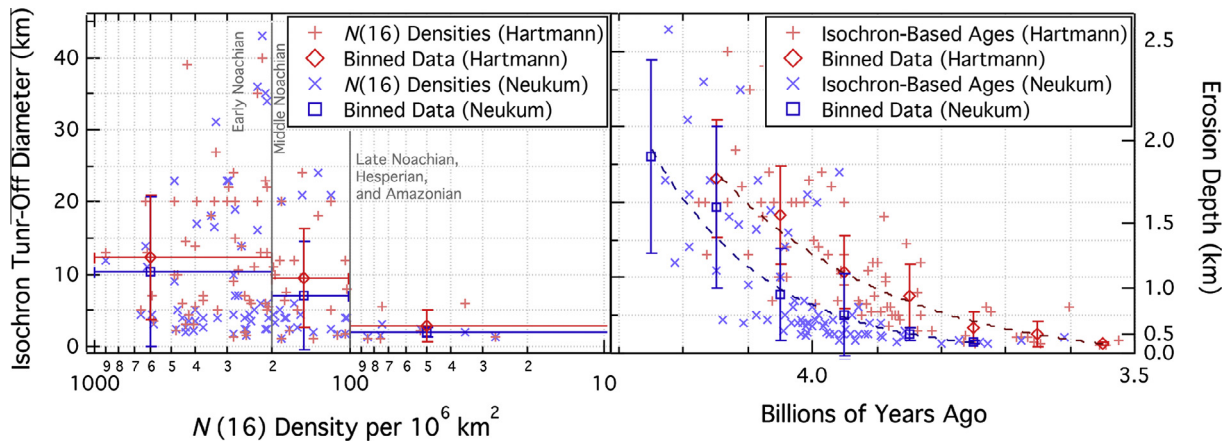


Fig. 6. Scatter plots showing the isochron turn-off diameter (left vertical axis) in each crater SFD as a function of $N(16)$ density (left) and model isochron age (right) with both chronologies. The corresponding fresh crater depth is on the right vertical axis (from Robbins and Hynes (2012)). Data on the left are binned by martian epoch; data on the right are binned in 100 Ma intervals. The temporal binning compares well between the two with the largest discrepancy between 4.0 and 4.1 Ga. A power-law fit through these (weighted by 1σ uncertainties) has an exponent of 16 ± 10 for Hartmann, 24 ± 9 for Neukum.

magnetic signature implies impact shock demagnetization of most of the basin, followed by the remagnetization of a central portion (either a melt sheet or a hydrothermal system) in a global dynamo magnetic field. In contrast, Prometheus is unambiguously demagnetized ($|B|_{185\text{km}} = 4.5 \text{ nT}$), as also discussed by Kletetschka et al. (2009).

The positions of the five dated basins (in this work: Isidis, Argyre, Hellas, Prometheus, Ladon) on a “magnetic timeline” are shown in Fig. 5 with both isochron and $N(50)$ ages. As discussed throughout this paper, the preferred age model is using the isochron method rather than $N(D)$, but both are presented for completeness. The non-unique $N(50)$ model ages of Ladon and Prometheus (55 ± 18 and 56 ± 21 , respectively) belie the possibility of assigning a definitive age for the cessation of the martian dynamo: The approximate center of the assigned ages is indicated with a dashed vertical line on the figure, and it is at approximately 4.09 Ga. The isochron-based ages are somewhat more distinct, though the formal error bars assigned do overlap. For Ladon, the Hartmann-based age is $4.07^{+0.05}_{-0.08}$ Ga versus $4.03^{+0.04}_{-0.05}$ Ga for Prometheus – a distinct overlap – while the Neukum-based ages are $4.18^{+0.05}_{-0.08}$ Ga and $4.07^{+0.03}_{-0.04}$ Ga, respectively – statistically distinct at the 1σ level. Using an average between the methods, the dynamo cessation is placed between 4.06 and 4.07 Ga, consistent with previous works and with the $N(50)$ given the uncertainty involved. Given that Ladon and Prometheus are similarly sized basins with a similar topographic expression and crustal thickness (Neumann et al., 2004), it is reasonable to suggest that the stark difference in their magnetic field strengths is reflective of very different global magnetic environments persisting at the times of their formation: Ladon in the presence of a global dynamo-driven magnetic field and Prometheus in the absence thereof.

Magnetic signatures of the large craters below $\sim 1000 \text{ km}$ in diameter were not examined because the non-unique relationship between subsurface magnetization and magnetic field is such that demagnetization signatures become increasingly obscured with altitude. In the martian case, particularly since the dominant coherence scale of subsurface magnetization on Mars is on the order of 600 km (Voorhies, 2008; Lillis et al., 2010), the demagnetized zone needs to be larger than $\sim 700 \text{ km}$ for a lack of magnetic field to unambiguously mean a lack of subsurface magnetization (Lillis et al., 2010).

With the caveats that (a) Ladon might be older than was dated with this method due to significant resurfacing and (b) the flux of impactors may not have been a smoothly decreasing function (e.g.,

Morbidelli et al., 2012), the ages determined imply a possibly rapid dynamo cessation, taking place on the order of a few 10s millions of years or less, around 4.06–4.09 Ga. Although this is slightly later (by 0.05 Gyr) than the similarly quick cessation suggested by Lillis et al. (2008a) using a different cratering chronology and different crater populations (QCDs and CTAs $> 300 \text{ km}$ in diameter), the story remains broadly consistent: a relatively sudden shift from craters cooling in a strong global magnetic field to those cooling in a much weaker or nonexistent field. The possibility that this dynamo cessation was due to the cumulative effect on core–mantle heat flux of many giant impactors was discussed by Roberts et al. (2009). Also, the lack of a global magnetic field likely increased atmospheric erosion through solar wind stripping (e.g., Jakosky et al., 1994) which may be responsible for a change in the geochemical alteration environment, from aqueous alteration forming phyllosilicates (“Phyllosian Era”) to hydrated sulfates and ferric oxides formed in a more acidic environment (“Theiikian Era”) (Bibring et al., 2007). This change occurred sometime before the Isidis impact (Mustard et al., 2007), which we place at 3.95–3.99 Ga (using isochrons). This atmospheric erosion hypothesis will be tested more fully with data from the MAVEN orbiter in 2014.

5.2. Crater obliteration rates

If one can assume that crater SFDs’ deviation from the isochron function is due to resurfacing, then plotting the diameter of this turn-off versus the feature’s age (in this case the large impact craters) should be an estimate for resurfacing rates through time. This is illustrated in Fig. 6, which shows these data graphed versus $N(16)$ density (to assign martian epochs) and isochron-based age; the data are listed in Tables 2 and 3 (online sup.). The diameter at which this deviation from the isochron happens is termed the “turn-off point.” Before the results are discussed, caution should be emphasized reading into any individual crater’s turn-off point, as well as turn-off points for some of the smallest craters: It is possible that, due to few large ($\sim 50 \text{ km}$) superposed craters on the smaller craters dated ($\sim 150 \text{ km}$), isochrons were fit to a later resurfacing age rather than the formation age, and the turn-off diameter is artificially small. Vinogradov (Fig. 7t) is an example. However, the results as a whole, especially those for larger craters, should be robust despite this issue.

The $N(16)$ (left) panel is less conclusive than the isochron-based ages (right), but both panels of Fig. 6 show the same trend of a

decreasing turn-off diameter with increasing age or increasing crater density. The $N(16)$ values are binned by martian epoch, and they show a significant decrease of erosion after the Middle Noachian time period ($N(16) < 100$). Coarsely, the isochron results can be binned into two groups of pre-3.8 and post-4.0 Ga from the Hartmann chronology and pre-3.9/post-4.1 Ga for the Neukum chronology. Under the Hartmann isochron-based ages, craters younger than ~ 3.8 Ga all have turn-off points $D < 10$ km. Those older than 4.0 Ga all have turn-off points $D > 10$ km. Similarly, under the Neukum-based system all craters younger than ~ 3.9 Ga have turn-offs $D < 10$ km, while those older than 4.1 Ga have turn-off points $D > 10$ km. As a general rule of thumb, fresh craters $D = 10$ km form with a depth $d \approx 1.1$ km (Robbins and Hynek, 2012). It can then be estimated that surfaces older than 4.1 Ga experienced ~ 1 km of resurfacing over the past 4.1 Ga, but that surfaces younger than 3.9 Ga experienced significantly less. This points toward a period of rapid resurfacing on the planet around the latter half of the Middle Noachian to the Late Noachian, in agreement with previous work (e.g., Craddock and Maxwell, 1993; Craddock and Howard, 2002; Forsberg-Taylor et al., 2004; Boyce and Garbeil, 2007; Hoke and Hynek, 2009), including the approximate amount of resurfacing or resurfacing rates proposed. These new results are an independent method of arriving at this conclusion, lending support for it and use of the method on other surfaces.

6. Conclusions

This new work presents uniform and comprehensive age-modeling results for 78 large craters on Mars, $\approx 78\%$ of which have not been previously dated in this extensive, uniform manner. We have used it to establish an impact probability function that shows a decrease in the number of large impacts since ~ 3.9 –4.0 Ga, and though it must be emphasized this is model-dependent (Hartmann (2005) or Neukum et al. (2001) chronology), it is an ensemble conclusion. If we used a chronology function that factored in an impact spike corresponding to the LHB, then our age distribution may reflect this. Ergo, if the LHB happened at Mars, then the time-scaling function converting $N(D)$ densities/isochron values (i.e., Ivanov, 2001) is incorrect and needs to be modified, pushing ages to younger times.

The ages we derived in general agree with previous works to within $\sim 2\sigma$ uncertainty (see Section 4.4 and Table 2). There are outliers from this comparison, and these can generally be explained by different mapping techniques and different diameter craters used for the dating. Within the dating systems, we found some significant differences with a lack of self-consistency between the two main systems – Hartmann (2005) and Neukum et al. (2001) – where ages derived from different $N(D)$ densities must disagree with each other, and using smaller diameter craters will almost always yield younger ages, likely due to resurfacing. From this work, if one must use $N(D)$ to estimate ages, we recommend using the largest diameter craters for which enough exist in order to derive statistically meaningful ages; these are the least likely craters to be removed and most likely to represent an accurate relative age. If possible, fitting isochrons to CSFD ranges that best parallel the chronology of choice will likely yield a more accurate age over the $N(D)$ method. We also recommend that future researchers be as explicit as possible when describing how their model ages were determined and why that method was used.

Making the assumption that the isochron ages are reasonably accurate at the ~ 100 Myr level, we applied the age results to resurfacing rates and Mars' magnetic core dynamo. Our results are consistent with previous work on the dynamo and constrain the cutoff to be between the formation of the Ladon and Prometheus basins.

We also showed via a new method that prior works suggesting rapid resurfacing on Mars around the Middle/Late Noachian transition fit well with SFD-isochron deviations. Additionally, Gale crater, the site of the *Mars Science Laboratory Curiosity*, is likely Noachian aged, dates to ~ 3.68 –3.89 Ga, and it was one of the last craters > 150 km in diameter to form on Mars.

Acknowledgments

Thanks to E.B. Bierhaus and H.V. Frey for providing detailed and helpful comments on the manuscript. Support for Robbins and Hynek was through NASA's Mars Data Analysis Program (MDAP) Award NNX10AL65G. Support for Lillis was through MDAP Award NNX11AI85G. Support for Bottke was provided by NASA's Lunar Science Institute (Center for Lunar Origin and Evolution, Grant Number NNA09DB32A) and by NSF's Planetary Astronomy Program.

Appendix A. Supplementary material

Supplementary data associated with this article can be found, in the online version, at <http://dx.doi.org/10.1016/j.icarus.2013.03.019>.

References

- Bibring, J.-P. et al., 2007. Coupled ferric oxides and sulfates on the martian surface. *Science* 317, 1206–1210. <http://dx.doi.org/10.1126/science.1144174>.
- Boyce, J.M., Garbeil, H., 2007. Geometric relationships of pristine martian complex impact craters, and their implications to Mars geologic history. *Geophys. Res. Lett.* 34, L16201. <http://dx.doi.org/10.1029/2007GL029731>.
- Cabrol, N.A., Grin, E.A., Newsom, H.E., Landheim, R., McKay, C.P., 1999. Hydrologic evolution of Gale crater and its relevance to the exobiological exploration of Mars. *Icarus* 139 (2), 235–245. <http://dx.doi.org/10.1006/icar.1999.6099>.
- Christensen, P.R. et al., 2004. The Thermal Emission Imaging System (THEMIS) for the Mars 2001 Odyssey Mission. *Space Sci. Rev.* 110 (1), 85–130. <http://dx.doi.org/10.1023/B:SPAC.0000021008.16305.94>.
- Craddock, R.A., Howard, A.D., 2002. The case for rainfall on a warm, wet early Mars. *J. Geophys. Res.* 107 (E11), 5111. <http://dx.doi.org/10.1029/2001JE001505>.
- Craddock, R.A., Maxwell, T.A., 1993. Geomorphic evolution of the martian highlands through ancient fluvial processes. *J. Geophys. Res.* 98 (E2), 3453–3468. <http://dx.doi.org/10.1029/92JE02508>.
- Crater Analysis Techniques Working Group (Arvidson, R. et al.), 1979. Standard techniques for presentation and analysis of crater size–frequency data. *Icarus* 37, 467–474.
- Edwards, C.S., Nowicki, K.J., Christensen, P.R., Hill, J., Gorelick, N., Murray, K., 2011. Mosaicking of global planetary image datasets: 1. Techniques and data processing for Thermal Emission Imaging System (THEMIS) multi-spectral data. *J. Geophys. Res.* 116, E10008. <http://dx.doi.org/10.1029/2010JE003755>.
- Fassett, C.I., Head, J.W., 2011. Sequence and timing of conditions on early Mars. *Icarus* 211, 1204–1214. <http://dx.doi.org/10.1016/j.icarus.2010.11.014>.
- Fassett, C.I. et al., 2012. Lunar impact basins: Stratigraphy, sequence and ages from superposed impact crater populations measured from Lunar Orbiter Laser Altimeter (LOLA) data. *J. Geophys. Res.* 117, E00H06. <http://dx.doi.org/10.1029/2011JE003951>.
- Forsberg-Taylor, N.K., Howard, A.D., Craddock, R.A., 2004. Crater degradation in the martian highlands: Morphometric analysis of the Sinus Sabaeus region and simulation modeling suggest fluvial processes. *J. Geophys. Res.* 109, E05002. <http://dx.doi.org/10.1029/2004JE002242>.
- Frey, H.V., 2004. A timescale for major events in early Mars crustal evolution. *Lunar Planet. Sci. Conf. Abstract* #1382.
- Frey, H.V., 2008. Ages of very large impact basins on Mars: Implications for the late heavy bombardment in the inner Solar System. *Geophys. Res. Lett.* 35, L13203. <http://dx.doi.org/10.1029/2008GL033515>.
- Greeley, R., Guest, J.E., 1987. Geologic Map of the Eastern Equatorial Region of Mars. USGS Misc. Inv. Series Map I-1802-B.
- Hartmann, W.K., 2005. Martian cratering 8: Isochron refinement and the chronology of Mars. *Icarus* 174, 294–320. <http://dx.doi.org/10.1016/j.icarus.2004.11.023>.
- Hoke, M.R.T., Hynek, B.M., 2009. Roaming zones of precipitation on ancient Mars as recorded in valley networks. *J. Geophys. Res.* 113, E8. <http://dx.doi.org/10.1029/2008JE003247>.
- Ivanov, B.A., 2001. Mars/Moon cratering rate ratio estimates. *Chronol. Evol. Mars* 96, 87–104.
- Jakosky, B.M., Pepin, R.O., Johnson, R.E., Fox, J.L., 1994. Mars atmospheric loss and isotopic fractionation by solar-wind-induced sputtering and photochemical escape. *Icarus* 111 (2), 271–288. <http://dx.doi.org/10.1006/icar.1994.1145>.

- Kletetschka, G., Lillis, R.J., Ness, N.F., Acuña, M.H., Connerney, J.E.P., Wasilewski, P.J., 2009. Magnetic zones of Mars: Deformation-controlled origin of magnetic anomalies. *Meteorit. Planet. Sci.* 44 (1), 131–140. <http://dx.doi.org/10.1111/j.1945-5100.2009.tb00723.x>.
- Lillis, R.J., Frey, H.V., Manga, M., 2008a. Rapid decrease in martian crustal magnetization in the Noachian era: Implications for the dynamo and climate of early Mars. *Geophys. Res. Lett.* 35, L14203. <http://dx.doi.org/10.1029/2008GL034338>.
- Lillis, R.J., Frey, H.V., Manga, M., Mitchell, D.L., Lin, R.P., Acuña, M.H., Bougher, S.W., 2008b. An improved crustal magnetic field map of Mars from electron reflectometry: Highland volcano magmatic history at the end of the martian dynamo. *Icarus* 194, 575–596. <http://dx.doi.org/10.1016/j.icarus.09.032>.
- Lillis, R.J. et al., 2010. Study of impact demagnetization at Mars using Monte Carlo modeling and multiple altitude data. *J. Geophys. Res.* 115, E07007. <http://dx.doi.org/10.1029/2009JE003556>.
- Michael, G.G., Neukum, G., 2010. Planetary surface dating from crater size–frequency distribution measurements: Partial resurfacing events and statistical age uncertainty. *Earth Planet. Sci. Lett.* 294, 223–229. <http://dx.doi.org/10.1016/j.epsl.2009.12.041>.
- Morbidelli, A., Marchi, S., Bottke, W.F., Kring, D.A., 2012. A sawtooth-like timeline for the first billion years of lunar bombardment. *Earth Planet. Sci. Lett.* 355–356, 144–151. <http://dx.doi.org/10.1016/j.epsl.2012.07.037>.
- Mustard, J.F. et al., 2007. Mineralogy of the Nili Fossae region with OMEGA/Mars Express data: 1. Ancient impact melt in the Isidis Basin and implications for the transition from the Noachian to Hesperian. *J. Geophys. Res.* 112, E8. <http://dx.doi.org/10.1029/2006JE002834>.
- Neukum, G., 1983. Meteoritenbombardement und Datierung planetarer Oberflächen. Habilitation Dissertation for Faculty Membership, Univ. of Munich. 186pp.
- Neukum, G., Ivanov, B.A., Hartmann, W.K., 2001. Cratering records in the inner Solar System in relation to the lunar reference system. *Chronol. Evol. Mars* 96, 55–86.
- Neumann, G.A., Zuber, M.T., Wieczorek, M.A., McGovern, P.J., Lemoine, F.G., Smith, D.E., 2004. Crustal structure of Mars from gravity and topography. *J. Geophys. Res.* 109, E8. <http://dx.doi.org/10.1029/2004JE002262>.
- Nimmo, F., Tanaka, K.L., 2005. Early crustal evolution of Mars. *Annu. Rev. Earth Planet. Sci.* 33, 133–161. <http://dx.doi.org/10.1146/annurev.earth.33.092203.122637>.
- Robbins, S.J., Hynek, B.M., 2011. Secondary crater fields from 24 large primary craters on Mars: Insights into nearby secondary crater production. *J. Geophys. Res.* 116, E10003. <http://dx.doi.org/10.1029/2011JE003820>.
- Robbins, S.J., Hynek, B.M., 2012. A new global database of Mars impact craters ≥ 1 km: 1. Database creation, properties, and parameters. *J. Geophys. Res.* 117, E05004. <http://dx.doi.org/10.1029/2011JE003966>.
- Roberts, J.H., Lillis, R.J., Manga, M., 2009. Giant impacts on early Mars and the cessation of the martian dynamo. *J. Geophys. Res.* 114, E04009. <http://dx.doi.org/10.1029/2008JE003287>.
- Schultz, R.A., Frey, H., 1990. A new survey of multiring impact basins on Mars. *J. Geophys. Res.* 90 (B9), 14175–14189. <http://dx.doi.org/10.1029/BJ095iB09p14175>.
- Schultz, P.H., Schultz, R.A., Rogers, J., 1982. The structure and evolution of ancient impact basins on Mars. *J. Geophys. Res.* 87 (B12), 9803–9820. <http://dx.doi.org/10.1029/JB087iB12p09803>.
- Smith, D.E. et al., 2001. Mars Orbiter Laser Altimeter: Experiment summary after the first year of global mapping of Mars. *J. Geophys. Res.* 106 (E10), 23689–23722. <http://dx.doi.org/10.1029/2000JE001364>.
- Solow, A.R., 2002. Estimating event rates in the presence of dating error with an application to lunar impacts. *Earth Planet. Sci. Lett.* 199, 1–6. [http://dx.doi.org/10.1016/S0012-821X\(20\)00541-1](http://dx.doi.org/10.1016/S0012-821X(20)00541-1).
- Stöffler, D., Ryder, G., 2001. Stratigraphy and isotope ages of lunar geologic units: Chronological standard for the inner Solar System. *Space Sci. Rev.* 96, 9–54.
- Strom, R.G., Malhotra, R., Ito, T., Yoshida, F., Kring, D.A., 2005. The origin of planetary impactors in the inner Solar System. *Science* 309, 1847–1850. <http://dx.doi.org/10.1126/science.1113544>.
- Tanaka, K.L., 1986. The stratigraphy of Mars. *J. Geophys. Res.* 91 (B13), E139–E158. <http://dx.doi.org/10.1029/JB091iB13p0E139>.
- Tanaka, K.L. et al., 2012. The geology of Mars: What the new global map shows. *Lunar Planet. Sci. Abstract* #2702.
- Thompson, B.J., Bridges, N.T., Milliken, R., Baldrige, A., Hook, S.J., Crowley, J.K., Marion, G.M., de Sousa Filho, C.R., Brown, A.J., Weitz, C.M., 2011. Constraints on the origin and evolution of the layered mound in Gale crater, Mars using Mars Reconnaissance Orbiter data. *Icarus* 214 (2), 413–432. <http://dx.doi.org/10.1016/j.icarus.2011.05.002>.
- Voorhies, C.V., 2008. Thickness of the magnetic crust of Mars. *J. Geophys. Res.* 113, E4. <http://dx.doi.org/10.1029/2007JE002928>.
- Werner, S.C., 2008. The early martian evolution – Constraints from basin ages. *Icarus* 195, 45–60. <http://dx.doi.org/10.1016/j.icarus.2007.12.008>.
- Werner, S.C., Tanaka, K.L., 2011. Redefinition of the crater-density and absolute-age boundaries for the chronostratigraphic system of Mars. *Icarus* 215, 603–607. <http://dx.doi.org/10.1016/j.icarus.2011.07.024>.
- Wilhelms, D.E., 1973. Comparison of martian and lunar multiringed circular basins. *J. Geophys. Res.* 78 (20), 4084–4095. <http://dx.doi.org/10.1029/JB078i020p04084>.